

Coordinate Translator for Learning Deformable Medical Image Registration

Yihao Liu¹, Lianrui Zuo^{1,2}, Shuo Han³, Jerry L. Prince¹, and Aaron Carass¹

¹ Department of Electrical and Computer Engineering,
Johns Hopkins University, Baltimore, MD 21218 USA

² Laboratory of Behavioral Neuroscience, National Institute on Aging,
National Institute of Health, Baltimore, MD 20892 USA

³ Department of Biomedical Engineering,
Johns Hopkins University, Baltimore, MD 21218 USA

Abstract. The majority of deep learning (DL) based deformable image registration methods use convolutional neural networks (CNNs) to estimate displacement fields from pairs of moving and fixed images. This, however, requires the convolutional kernels in the CNN to not only extract intensity features from the inputs but also understand image coordinate systems. We argue that the latter task is challenging for traditional CNNs, limiting their performance in registration tasks. To tackle this problem, we first introduce Coordinate Translator (CoTr), a differentiable module that identifies matched features between the fixed and moving image and outputs their coordinate correspondences without the need for training. It unloads the burden of understanding image coordinate systems for CNNs, allowing them to focus on feature extraction. We then propose a novel deformable registration network, **im2grid**, that uses multiple CoTr’s with the hierarchical features extracted from a CNN encoder and outputs a deformation field in a coarse-to-fine fashion. We compared **im2grid** with the state-of-the-art DL and non-DL methods for unsupervised 3D magnetic resonance image registration. Our experiments show that **im2grid** outperforms these methods both qualitatively and quantitatively.

Keywords: Deformable Image Registration · Deep Learning · Magnetic Resonance Imaging · Template Matching.

1 Introduction

Deformable registration is of fundamental importance in medical image analysis. Given a pair of images, one fixed and one moving, deformable registration warps the moving image by optimizing the parameters of a nonlinear transformation so that the underlying anatomies of the two images are aligned according to an image dissimilarity function [11, 15, 27, 28, 31]. Recent deep learning (DL) methods use convolutional neural networks (CNNs) whose parameters are optimized during training; at test time, a dense displacement field that represents the deformable transformation is generated in a single forward pass.

Although CNN-based methods for segmentation and classification are better than traditional methods in both speed and accuracy, DL-based deformable registration methods are faster but not more accurate [5, 8, 13, 14, 32]. Using a CNN for registration requires learning coordinate correspondences between image pairs, which has been thought to be fundamentally different from other CNN applications because it involves both extracting and matching features [2, 20]. However, the majority of existing works simply rely on CNNs to implicitly learn the displacement between the fixed and moving images [5, 13, 14].

Registration involves both feature extraction and feature matching, but to produce a displacement field, matched features need to be translated to coordinate correspondences. We argue that using convolutional kernels for the latter two tasks is not optimal. To tackle this problem, we introduce Coordinate Translator (CoTr), a differentiable module that matches features between the fixed and moving images and identifies feature matches as precise coordinate correspondences without the need for training. The proposed registration network, named **im2grid**, uses multiple CoTr’s with multi-scale feature maps. These produce multi-scale sampling grids representing coordinate correspondences, which are then composed in a coarse-to-fine manner to warp the moving image. **im2grid** explicitly handles the task of matching features and establishing coordinate correspondence using CoTr’s, leaving only feature extraction to our CNN encoder.

Throughout this paper, we use the unsupervised 3D magnetic resonance (MR) image registration as our example task and demonstrate that the proposed method outperforms the state-of-the-art methods in terms of registration accuracy. We think it is important to note that because producing a coordinate location is such a common task in both medical image analysis and computer vision, the proposed method can be impactful on a board range of applications.

2 Related Works

Traditional registration methods solve an optimization problem for every pair of fixed I_f and moving I_m images. Let ϕ denote a transformation and let the best transformation $\hat{\phi}$ be found from

$$\hat{\phi} = \arg \min_{\phi} L_{\text{sim}}(I_f, I_m \circ \phi) + \lambda L_{\text{smooth}}(\phi), \quad (1)$$

where $I_m \circ \phi$ yields the warped image I_w . The first term focuses on the similarity between I_f and $I_m \circ \phi$ whereas the second term—weighted by the hyperparameter λ —regularizes ϕ . The choice of L_{sim} is application-specific. Popular methods using this framework include spline-based free-form deformable models [27], elastic warping methods [11, 22], biomechanical models [15], and Demons [28, 31]. Alternatively, learning-based methods have also been used to estimate the transformation parameters [9, 17].

Recently, deep learning (DL) methods, especially CNNs, have been used for solving deformable registration problems. In these methods, ϕ is typically represented as a map of displacement vectors that specify the voxel-level spatial

offsets between I_f and I_m ; the CNN is trained to output ϕ with or without supervision [5, 7, 13, 14, 18]. In the unsupervised setting, the displacement field is converted to a sampling grid and the warped image is produced by using a grid sampler [21] with the moving image and the sampling grid as input. The grid sampler performs differentiable sampling of an image (or a multi-channel feature map) using a sampling grid; it allows the dissimilarity loss computed between the warped and fixed images to be back-propagated so the CNN can be trained end-to-end. In past work, [5] used a U-shaped network to output the dense displacement; [12, 13] used an encoder network to produce a sparse map of control points and generated the dense displacement field by interpolation; and [8] replaced the bottleneck of a U-Net [26] with a transformer structure [30]. Several deep learning methods also demonstrate the possibility of using a velocity-based transformation representation to enforce a diffeomorphism [10, 32].

Our method represents the transformation using a sampling grid G , which can be directly used by the grid sampler. For N -dimensional images ($N = 3$ in this paper), G is represented by an N -channel map. Specifically, for voxel coordinate $\mathbf{x} \in \mathbb{D}^N$ (where \mathbb{D}^N contains all the voxel coordinates in I_f), $G(\mathbf{x})$ should ideally hold a coordinate such that the two values $I_f(\mathbf{x})$ and $I_m(G(\mathbf{x}))$ represent the same anatomy. Note that a displacement field representation can be found as $\text{DF} = G - G_I$, where G_I is the identity grid $G_I(\mathbf{x}) = \mathbf{x}$.

3 Method

For the image pair I_f and I_m , the proposed method produces a sampling grid G_0 that can be used by the grid sampler to warp I_m to match I_f . Similar to previous DL methods, we use a CNN encoder to extract multi-level feature maps from I_f and I_m . Instead of directly producing a single displacement field from the CNN, G_0 is the composition of multi-level sampling grids, generated from the multi-level feature maps with the proposed Coordinate Translators (CoTr's).

3.1 Coordinate Translator

Let F and M denote the multi-channel feature maps that are individually extracted from I_f and I_m , respectively. A CoTr takes as input both F and M , and produces a sampling grid G that aligns M interpolated at coordinate $G(\mathbf{x})$ to $F(\mathbf{x})$ for all $\mathbf{x} \in \mathbb{D}^N$. For every \mathbf{x} , cross-correlation is calculated between $F(\mathbf{x})$ and $M(\mathbf{c}_i)$ along the feature dimension, where $\mathbf{c}_i \in \mathbb{D}^N$ for $i \in [1, K]$ are a set of candidate coordinates. The results are a K -element vector of matching scores between $F(\mathbf{x})$ and every $M(\mathbf{c}_i)$:

$$\text{Matching Score}(\mathbf{x}) = (F(\mathbf{x})^T M(\mathbf{c}_1), \dots, F(\mathbf{x})^T M(\mathbf{c}_K)). \quad (2)$$

The choice of \mathbf{c}_i 's determines the search region for the match. For example, defining \mathbf{c}_i to be every coordinates in \mathbb{D}^N will compare $F(\mathbf{x})$ against every location in M ; these matches can also be restricted within the $3 \times 3 \times 3$ neighborhood of

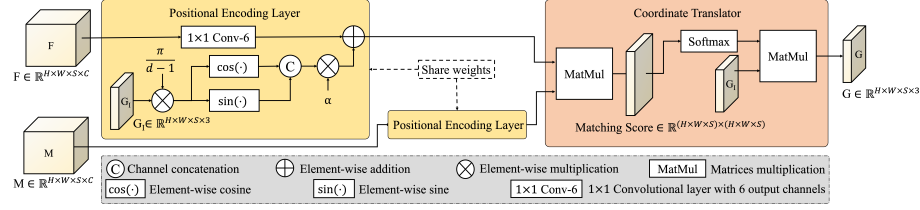


Fig. 1. Structure of the proposed positional encoding layer and Coordinate Translator.

\mathbf{x} . We outline our choices of \mathbf{c}_i 's in Sec. 4. The matching scores are normalized using a softmax function to produce a matching probability p_i ,

$$p_i = \frac{\exp(F(\mathbf{x})^T M(\mathbf{c}_i))}{\sum_j \exp(F(\mathbf{x})^T M(\mathbf{c}_j))} \quad \text{for every } \mathbf{c}_i. \quad (3)$$

We interpret the matching probabilities as the strength of attraction between $F(\mathbf{x})$ and $M(\mathbf{c}_i)$'s. Importantly, we can calculate a weighted sum of \mathbf{c}_i 's to produce a coordinate $\mathbf{x}' \in \mathbb{R}^N$, i.e., $\mathbf{x}' = \sum_{i=1}^K p_i \cdot \mathbf{c}_i$, which represents the correspondence of \mathbf{x} in the moving image I_m . This is conceptually similar to the combined force in the Demons algorithm [28]. For every $\mathbf{x} \in \mathbb{D}^N$ the corresponding \mathbf{x}' forms the CoTr output, G .

CoTr can be efficiently implemented as the Scaled Dot-Product Attention introduced in [30] using matrix operations. For 3D images with spatial dimension $H \times W \times S$ and C feature channels, we reshape F and M to $\mathbb{R}^{(H \times W \times S) \times C}$ and G_I to $\mathbb{R}^{(H \times W \times S) \times 3}$. Thus CoTr with $\{\mathbf{c}_1, \dots, \mathbf{c}_K\} = \mathbb{D}^N$ can be readily computed from,

$$\text{CoTr}(F, M) = \text{Softmax}(FM^T)G_I, \quad (4)$$

with the softmax operating on the rows of FM^T .

Positional encoding layer In learning transformations, it is a common practice to initialize from (or close to) an identity transformation [5, 8, 21]. As shown in Fig. 1, we propose a positional encoding layer that combines position information with F and M such that the initial output of CoTr is an identity grid. Inside a positional encoding layer, for every $\mathbf{x} = (x_1, \dots, x_N)$ with x_i 's on an integer grid ($x_i \in \{0, \dots, d_i - 1\}$), we add a positional embedding (PE),

$$\text{PE}(\mathbf{x}) = \left(\cos \frac{x_1 \pi}{d_1 - 1}, \sin \frac{x_1 \pi}{d_1 - 1}, \dots, \cos \frac{x_N \pi}{d_N - 1}, \sin \frac{x_N \pi}{d_N - 1} \right),$$

to the input feature map. Trigonometric identities give the cross-correlation of PEs at \mathbf{x}_1 and \mathbf{x}_2 as

$$\text{PE}(\mathbf{x}_1)^T \text{PE}(\mathbf{x}_2) = \sum_{i=1}^N \cos \left(\frac{\Delta x_i \pi}{d_i - 1} \right),$$

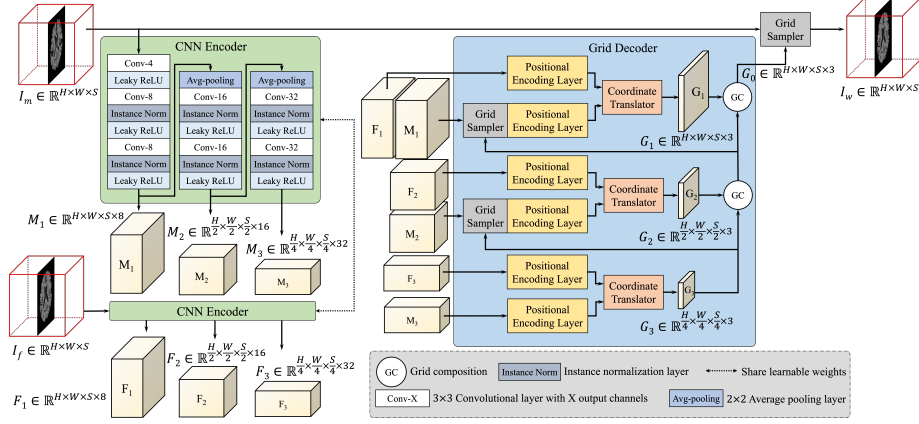


Fig. 2. Example of the proposed **im2grid** network structure with a 3-level CNN encoder.

where Δx_i is the difference in the i^{th} components of \mathbf{x}_1 and \mathbf{x}_2 . This has maximum value when $\mathbf{x}_1 = \mathbf{x}_2$ and decreases with the L_1 distance between the two coordinates. We initialize the convolutional layer to have zero weights and bias and the learnable parameter $\alpha = 1$ (see Fig. 1) such that only the PEs are considered by CoTr at the beginning of training. As a result, among all $\mathbf{c}_i \in \mathbb{D}^N$, $M(\mathbf{x})$ will have the highest matching score with $F(\mathbf{x})$, thus producing G_I as the initial output. CoTr also benefits from incorporating the position information as it allows the relative distance between \mathbf{c}_i and \mathbf{x} to contribute to the matching scores [30].

3.2 im2grid Network Architecture

The proposed **im2grid** network is shown in Fig. 2. Similar to previous methods, **im2grid** produces a sampling grid to warp I_m to I_w . Our CNN encoder uses multiple pooling layers to extract hierarchical features from the intensity images. In the context of intra-modal registration, it is used as a Siamese network that processes I_f and I_m separately. Figure 2 shows a three level **im2grid** model with three level feature maps $F_1/F_2/F_3$ and $M_1/M_2/M_3$ for I_f and I_m , respectively. Our grid decoder uses the common coarse-to-fine strategy in registration. Firstly, coarse features F_3 and M_3 are matched and translated to a coarse sampling grid G_3 using a CoTr. Because of the pooling layers, this can be interpreted as matching downsampled versions of I_f and I_m , producing a coarse displacement field. G_3 is then used to warp M_2 , resolving the coarse deformation between M_2 and F_2 so that the CoTr at the second level can capture more detailed displacements with a smaller search region. Similarly, M_1 is warped by the composed transformation of G_3 and G_2 and finally the moving image is warped by the composition of the transformations from all levels. A visualization of a five-level version of our multi-scale sampling grids is provided in Fig. 3. In contrast to previous methods that use CNNs to directly output displacements, our CNN encoder only need to

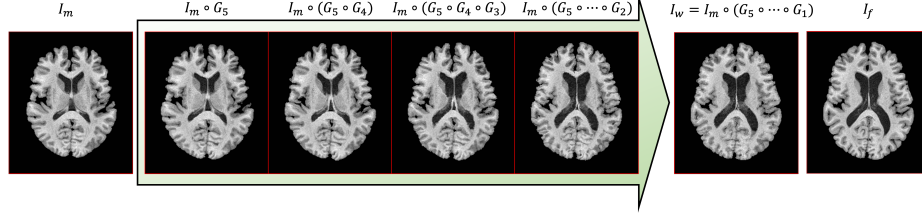


Fig. 3. Visualization of the multi-scale sampling grids by sequentially applying finer grids to the moving image, where we used a five-level CNN encoder and $G_5 \dots G_1$ are coarse to fine sampling grids produced from five-level feature maps.

extract similar intensity features for corresponding anatomies in I_f and I_m and the exact coordinate correspondences are obtained by CoTr's. Because our CNN encoder processes I_f and I_m separately, it is guaranteed that our CNN encoder only performs feature extraction.

The proposed network is trained using the mean squared difference between I_f and $I_w (= I_m \circ \phi)$ and a smoothness loss that regularizes the spatial variations of the G 's at every level,

$$\mathcal{L} = \frac{1}{|\mathbb{D}^N|} \sum_{\mathbf{x} \in \mathbb{D}^N} (I_f(\mathbf{x}) - I_w(\mathbf{x}))^2 + \lambda \sum_i \sum_{\mathbf{x} \in \mathbb{D}^N} \|\nabla(G_i(\mathbf{x}) - G_I(\mathbf{x}))\|^2, \quad (5)$$

where $|\mathbb{D}^N|$ is the cardinality of \mathbb{D}^N and all G_i 's and G_I are normalized to $[-1, 1]$.

4 Experiments

Datasets We used the publicly available OASIS3 [23] and IXI [1] datasets in our experiments. 200, 40, and 100 T1-weighted (T1w) MR images of the human brain from the OASIS3 dataset were used for training, validation, and testing, respectively. During training, two scans were randomly selected as I_f and I_m , while validation and testing used 20 and 50 pre-assigned image pairs, respectively. For the IXI dataset, we used 200 scans for training, 20 and 40 pairs for validation and testing, respectively. All scans underwent N4 inhomogeneity correction [29], and were rigidly registered to MNI space [16] with 1 mm^3 (for IXI) or 0.8 mm^3 (for OASIS3) isotropic resolution. A white matter peak normalization [25] was applied to standardize the MR intensity scale.

Evaluation Metrics First, we calculated the Dice similarity coefficient (DSC) between segmentation labels of I_f and the warped labels of I_m . An accurate transformation should align the structures of the fixed and moving images and produces a high DSC. We obtained a whole brain segmentation for the fixed and moving images using SLANT [19] and combined the SLANT labels (133 labels) to TOADS labels (9 labels) [6]. The warped labels were produced by applying each

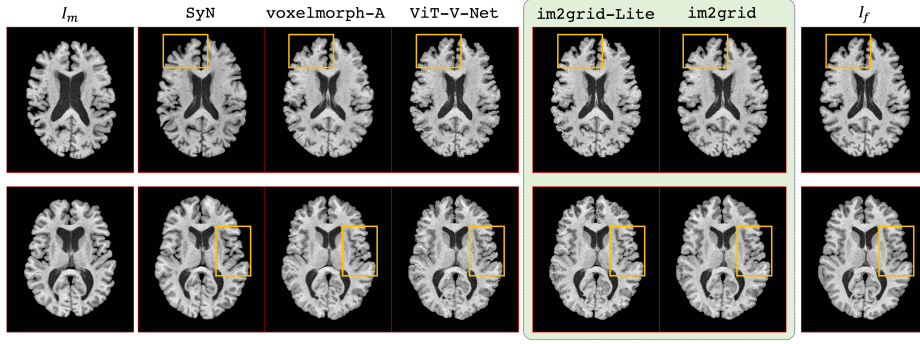


Fig. 4. Examples of registering the moving image (the first column) to the fixed image (the last column) using SyN, voxelmorph-A, ViT-V-Net, and our proposed methods.

methods deformation field to the moving image labels. Second, we measured the regularity of the transformations by computing the determinant of the Jacobian matrix, which should be globally positive for a diffeomorphic transformation.

Implementation Details Our method was implemented using PyTorch and trained using the Adam optimizer with a learning rate of 3×10^{-4} , a weight decay of 1×10^{-9} , and a batch size of 1. Random flipping of the input volumes along the three axes were used as data augmentation. We used a five-level structure and tested different choices of c_i 's for each CoTr. We found that given the hierarchical structure, a small search region at each level is sufficient to capture displacements presented in our data. Therefore, we implemented two versions of our method: 1) **im2grid** which used a 3×3 search window in the axial plane for producing G_1 and a $3 \times 3 \times 3$ search window at other levels; and 2) **im2grid-Lite** which is identical to **im2grid** except that the finest grid G_1 is not used.

Baseline Methods : We compared our method with several state-of-the-art DL and non-DL registration methods: 1) **SyN**: Symmetric image normalization method [3], implemented in the Advanced Normalization Tools (ANTs) [4]; 2) **voxelmorph-A**: The original implementation of voxelmorph with the mean squared error loss [5]; 3) **voxelmorph-B**: voxelmorph with hyper-parameter tuning; 4) **ViT-V-Net**: A transformer [30] based network structure proposed in [8].

For SyN, a wide range of hyper-parameters were tested on the OASIS3 validation set and the best performing parameters were used for generating the final results. For voxelmorph-B and ViT-V-Net, we adopted the same training strategies as the proposed method, including the loss function and data augmentation. We optimize the parameters of each method for performance on the OASIS3 validation set and then used those parameters in testing on both datasets.

Table 1. The Dice coefficient (DSC) and the percentage of voxels with positive determinant of Jacobian $|J_\phi| > 0$ for affine transformation, **SyN**, **Voxelmorph-A**, **Voxelmorph-B**, **ViT-V-Net**, and the proposed methods. The results of the initial alignment by the preprocessing steps are also included. Bold numbers indicate the best DSC for each dataset.

	OASIS3		IXI	
	DSC	$ J_\phi > 0$	DSC	$ J_\phi > 0$
Initial	0.651 ± 0.094	—	0.668 ± 0.107	—
Affine	0.725 ± 0.068	—	0.748 ± 0.052	—
SyN [3]	0.866 ± 0.029	100%	0.845 ± 0.035	100%
Voxelmorph-A [5]	0.878 ± 0.036	98.4%	0.834 ± 0.071	99.7%
Voxelmorph-B	0.883 ± 0.040	99.2%	0.842 ± 0.068	99.8%
ViT-V-Net [8]	0.872 ± 0.042	99.1%	0.845 ± 0.068	99.8%
im2grid-Lite	0.909 ± 0.021	100%	0.870 ± 0.043	100%
im2grid	0.908 ± 0.023	100%	0.865 ± 0.050	100%

Results For both OASIS3 and IXI test datasets, we registered the moving to the fixed image and report the averaged DSC for all labels in Table 1. In both datasets, the proposed methods outperform the comparison methods for DSC. For each individual anatomic label, we also conducted a paired, two-sided Wilcoxon signed rank test (null hypothesis: the difference between paired values comes from a distribution with zero median, $\alpha = 10^{-3}$) between our methods and the comparison methods. Both proposed methods show significant DSC improvements for seven of nine labels and comparable DSC performance to the best comparison method for the remaining two labels (thalamus and putamen). Interestingly, the proposed methods produced diffeomorphic transformations in all the experiments without an explicit diffeomorphism constraint (see comment in the Discussion). Visual examples on OASIS3 data are shown in Fig. 4. It can be seen, especially from the highlighted regions, that the warped image produced by the proposed methods have a better agreement with the fixed image.

5 Discussion

In this paper, we proposed CoTr for producing coordinate correspondences from two feature maps. Additionally, we proposed the im2grid network that uses CoTr’s for deformable image registration. For unsupervised 3D magnetic resonance registration, im2grid outperforms the state-of-the-art methods in accuracy with a similar training and testing speed as other deep learning based registration methods. Despite im2grid having no explicit guarantee of being diffeomorphic, it was experimentally found to be so for all cases. We believe this comes from our design decision to restrict the candidate voxels to the immediate neighborhood of a voxel at each level of our framework, which yields a composition of transformations that are locally linear and of decreasing size and therefore a diffeomorphism [24].

For registration, we demonstrated that using CoTr for matching features and establishing coordinate correspondences and the convolutional networks for fea-

ture extraction can significantly boost the performance. CoTr is a general module that can be incorporated in many existing network structures and therefore is not limited to the registration task. We believe that many tasks that involve image input and coordinate output can benefit from use of the CoTr module.

Acknowledgement This work was supported in part by the NIH/NEI grant R01-EY032284 and the Intramural Research Program of the NIH, National Institute on Aging.

References

1. IXI Brain Development Dataset. <https://brain-development.org/ixi-dataset/>
2. A. Dosovitskiy, A., et al.: FlowNet: Learning optical flow with convolutional networks. In: Proceedings of the IEEE International Conference on Computer Vision. pp. 2758–2766 (2015)
3. Avants, B.B., Epstein, C.L., Grossman, M., Gee, J.C.: Symmetric diffeomorphic image registration with cross-correlation: evaluating automated labeling of elderly and neurodegenerative brain. *Medical Image Analysis* **12**(1), 26–41 (2008)
4. Avants, B.B., Tustison, N., Song, G., et al.: Advanced normalization tools (ANTS). *Insight j* **2**(365), 1–35 (2009)
5. Balakrishnan, G., Zhao, A., Sabuncu, M.R., Guttag, J., Dalca, A.V.: Voxelmorph: a learning framework for deformable medical image registration. *IEEE Transactions on Medical Imaging* **38**(8), 1788–1800 (2019)
6. Bazin, P.L., Pham, D.L.: Topology-preserving tissue classification of magnetic resonance brain images. *IEEE Transactions on Medical Imaging* **26**(4), 487–496 (2007)
7. Cao, X., Yang, J., Zhang, J., Nie, D., Kim, M., Wang, Q., Shen, D.: Deformable image registration based on similarity-steered CNN regression. In: International Conference on Medical Image Computing and Computer-Assisted Intervention. pp. 300–308. Springer (2017)
8. Chen, J., He, Y., Frey, E.C., Li, Y., Du, Y.: ViT-V-Net: Vision transformer for unsupervised volumetric medical image registration. *arXiv preprint arXiv:2104.06468* (2021)
9. Chou, C.R., Frederick, B., Mageras, G., Chang, S., Pizer, S.: 2D/3D image registration using regression learning. *Computer Vision and Image Understanding* **117**(9), 1095–1106 (2013)
10. Dalca, A.V., Balakrishnan, G., Guttag, J., Sabuncu, M.R.: Unsupervised learning for fast probabilistic diffeomorphic registration. In: International Conference on Medical Image Computing and Computer-Assisted Intervention. pp. 729–738. Springer (2018)
11. Davatzikos, C.: Spatial transformation and registration of brain images using elastically deformable models. *Computer Vision and Image Understanding* **66**(2), 207–222 (1997)
12. De Vos, B.D., Berendsen, F.F., Viergever, M.A., Sokooti, H., Staring, M., Išgum, I.: A deep learning framework for unsupervised affine and deformable image registration. *Medical Image Analysis* **52**, 128–143 (2019)
13. de Vos, B.D., Berendsen, F.F., Viergever, M.A., Staring, M., Išgum, I.: End-to-end unsupervised deformable image registration with a convolutional neural network. In: Deep learning in medical image analysis and multimodal learning for clinical decision support, pp. 204–212. Springer (2017)

14. Fan, J., Cao, X., Yap, P.T., Shen, D.: BIRNet: Brain image registration using dual-supervised fully convolutional networks. *Medical Image Analysis* **54**, 193–206 (2019)
15. Ferrant, M., Warfield, S.K., Nabavi, A., Jolesz, F.A., Kikinis, R.: Registration of 3D intraoperative MR images of the brain using a finite element biomechanical model. In: *International Conference on Medical Image Computing and Computer-Assisted Intervention*. pp. 19–28. Springer (2000)
16. Fonov, V., Evans, A., McKinsty, R., Alml, C., Collins, D.: Unbiased nonlinear average age-appropriate brain templates from birth to adulthood. *NeuroImage* **47**, S102 (2009)
17. Gutiérrez-Becker, B., Mateus, D., Peter, L., Navab, N.: Learning optimization updates for multimodal registration. In: *International Conference on Medical Image Computing and Computer-Assisted Intervention*. pp. 19–27. Springer (2016)
18. Han, R., et al.: Deformable MR-CT image registration using an unsupervised end-to-end synthesis and registration network for endoscopic neurosurgery. In: *Medical Imaging 2021*. vol. 11598, p. 1159819. International Society for Optics and Photonics (2021)
19. Huo, Y., Xu, Z., Xiong, Y., Aboud, K., Parvathaneni, P., Bao, S., Bermudez, C., Resnick, S.M., Cutting, L.E., Landman, B.A.: 3D whole brain segmentation using spatially localized atlas network tiles. *NeuroImage* **194**, 105–119 (2019)
20. Ilg, E., et al.: FlowNet 2.0: Evolution of optical flow estimation with deep networks. In: *Proceedings of the IEEE Conference on Computer Vision and Pattern Recognition*. pp. 2462–2470 (2017)
21. Jaderberg, M., Simonyan, K., Zisserman, A., et al.: Spatial transformer networks. *Advances in Neural Information Processing Systems* **28** (2015)
22. Klein, S., Staring, M., Murphy, K., Viergever, M.A., Pluim, J.P.: Elastix: a toolbox for intensity-based medical image registration. *IEEE Transactions on Medical Imaging* **29**(1), 196–205 (2009)
23. LaMontagne, P.J., Benzinger, T.L., Morris, J.C., Keefe, S., Hornbeck, R., Xiong, C., Grant, E., Hassenstab, J., Moulder, K., Vlassenko, A.G., et al.: OASIS-3: longitudinal neuroimaging, clinical, and cognitive dataset for normal aging and alzheimer disease. *MedRxiv* (2019)
24. Narayanan, R., Fessler, J.A., Park, H., Meyer, C.R.: Diffeomorphic Nonlinear Transformations: A Local Parametric Approach for Image Registration. In: *19th Inf. Proc. in Med. Imaging (IPMI 2005)*. Lecture Notes in Computer Science, vol. 3565, pp. 174–185 (2005)
25. Reinhold, J.C., et al.: Evaluating the impact of intensity normalization on MR image synthesis. In: *Medical Imaging 2019: Image Processing*. vol. 10949, p. 109493H. International Society for Optics and Photonics (2019)
26. Ronneberger, O., Fischer, P., Brox, T.: U-Net: Convolutional networks for biomedical image segmentation. In: *International Conference on Medical image computing and computer-assisted intervention*. pp. 234–241. Springer (2015)
27. Rueckert, D., Sonoda, L.I., Hayes, C., Hill, D.L., Leach, M.O., Hawkes, D.J.: Nonrigid registration using free-form deformations: application to breast MR images. *IEEE Transactions on Medical Imaging* **18**(8), 712–721 (1999)
28. Thirion, J.P.: Image matching as a diffusion process: an analogy with maxwell’s demons. *Medical Image Analysis* **2**(3), 243–260 (1998)
29. Tustison, N.J., Avants, B.B., Cook, P.A., Zheng, Y., Egan, A., Yushkevich, P.A., Gee, J.C.: N4ITK: improved N3 bias correction. *IEEE Transactions on Medical Imaging* **29**(6), 1310–1320 (2010)

30. Vaswani, A., Shazeer, N., Parmar, N., Uszkoreit, J., Jones, L., Gomez, A.N., Kaiser, Ł., Polosukhin, I.: Attention is all you need. *Advances in Neural Information Processing Systems* **30** (2017)
31. Vercauteren, T., Pennec, X., Perchant, A., Ayache, N.: Diffeomorphic demons: Efficient non-parametric image registration. *NeuroImage* **45**(1), S61–S72 (2009)
32. Yang, X., Kwitt, R., Styner, M., Niethammer, M.: Quicksilver: Fast predictive image registration—a deep learning approach. *NeuroImage* **158**, 378–396 (2017)